Image-Based Robust Adaptive Fuzzy Control for Robots with Guaranteed Field of View and Uncertain Dynamics

Jiao Jiang, Yaonan Wang, Yiming Jiang, Yun Feng, Hang Zhong, Chenguang Yang

November 21, 2023

Abstract

Visual servoing technology has widely been employed in manufacturing because it is a flexible, realizability, and low-cost way to improve the intelligence of the industry robot. Nevertheless, a worrisome and overlooked issue is that the loss of visual features in the camera's field of view may lead to the failures of the visual servoing tasks. This article addresses the visual features escaping problem, by implementing an asymmetric barrier Lyapunov function with a field of view constraint controller. The asymmetric barrier Lyapunov function defines a tightly specified range for the feature coordinate errors and ensures the transient response of the tracking error as well as enables arbitrary tracking accuracy. It is worth noting that the asymmetric barrier Lyapunov function directly handles the visual-robot coupled dynamics while guaranteeing system stabilities. Besides, to accommodate the uncertain dynamics derived from a high-dimensional coupled system, an adaptive controller is proposed utilizing fuzzy neural networks with computational efficiency and few training parameters to enhance the control performance. Finally, the effectiveness of the proposed control strategy has been demonstrated through both theoretical analysis and experimental verification.

Keywords: Visual servoing, fuzzy neural networks, field of view constraints, asymmetric barrier Lyapunov function.

1 Introduction

In recent years, visual servoing technology has been proposed and widely applied in various areas, for instance, logistics robots, service robots, surgical robots, and industrial robots [4, 17, 34, 44], as shown in Fig.1. The visual servoing controller can be summarized into three categories. Based on the difference of the control input variables, visual servoing can be divided into Image-Based Visual Servoing (IBVS) and Position-Based Visual Servoing (PBVS) [3]. Combining 3D pose and 2D image feature signals as control input variables are defined as Hybrid Visual Servoing (HVS) [25].

The PBVS method relies on the 3D position of the camera to regulate the pose of the end-effector in Cartesian space, which is applicable for industrial robotic manipulators due to its attribute of global asymptotic stability. Nevertheless, the PBVS approach makes it hard to achieve high precision control owing to it being inevitably impacted by camera calibration errors as well as robot modeling errors. In contrast, IBVS directly utilizes image feature variables as the control input, which avoids the disadvantage of PBVS and can achieve accurate control.

In this paper, an IBVS control scheme is considered under an eye-in-hand system. The implementation of the IBVS task directly relies on the minimization of the error between the desired and the current image features. Thus, ensuring that the visual features remain within the camera's field of view (FoV) is a hard requirement, and also crucial to ensure that the visual servoing task is completed. If some visual features vanish from the camera's FoV, it will lead to the failure of visual servoing. As is well known that at least four visual features are required to ensure the IBVS task success [3].

To retain the visual features to stay within the FoV of the camera, many researchers have made great efforts to handle this. In [29], the FoV constraint problem of visual servoing is implicitly expressed as an optimal a control problem by combining demonstration learning and DMP to obtain the best control performance. Huang et al. [13] designed a constrained controller with a control barrier function and quadratic programming to prevent visual feature escape from FoV. Several scholars addressed the visual field visibility problem utilizing active vision techniques. Garcia-Aracil et al. [5] by reducing the weight of visual features that are about to escape from the camera's FoV to mitigate the impact of some vanishing visual features on the visual servoing task. Xin et al. [39], using a zooming camera to handle the vision visibility problem, combined with a depth adaptive zooming control strat-

This work was supported in part by the National Natural Science Foundation of China under Grants 62293510, 62293515, 62003136, 62203161; the Special funding support for the construction of innovative provinces in Hunan Province under Grant 2021GK1010; the Open Research Fund from Guangdong Laboratory of Artificial Intelligence and Digital Economy (SZ) (GML-KF-22-14).

Jiao Jiang, Yaonan Wang, and Yun Feng are with the College of Electrical and Information Engineering, Hunan University, Changsha 410082, China (e-mail: jiangjiao@hnu.edu.cn; yaonan@hnu.edu.cn; fyrobot@hnu.edu.cn).

Yiming Jiang and Hang Zhong are with the College of Robotics, Hunan University, Changsha 410082, China (e-mail: ymjiang@hnu.edu.cn; zhonghang@hnu.edu.cn).

Chenguang Yang is with the Bristol Robotics Laboratory, University of the West of England, Bristol BS16 1QY, U.K. (e-mail: cyang@ieee.org).

(a) (b)

Figure 1: Real scenarios of visual servoing applications. (a) Engine blade assembly. (b) Engine cylinder assembly.

egy to dynamically adapt to the change of the camera's FoV. Nonetheless, the main drawback of the above tactics is that a minimum number of visual features is not guaranteed, imperiling visual servoing task success. Another approach to manage FoV constraints with path planning [1, 9, 10, 18, 19, 38, 43]. Wang et al. [38] developed a virtual-goal-guided rapidly-exploring random tree (RRT) approach to handle the FoV visibility problem. In [1,10,43], the FoV constraints are handled by employing Model Predictive Control to generate the reference trajectory and camera velocity of the visual servoing task. In [18], a randomized kinodynamic path planning algorithm is proposed to generate desired feature trajectories in image space. Keshmiri et al. [19] developed a semi-offline trajectory planning approach to ease the limitation of the FoV of the camera. The deficiencies of the path planning schemes are that they are time-consuming for resolving the optimization reference trajectory and hard to implement for real platforms. Hence, in [2, 8], Bechlioulis et al. considered a prescribed performance control (PPC) solution to satisfy FoV constraints, by applying error transformation that imposes preordained transient and steady-state response on the visual feature coordinate errors. Miao et al. [27] utilizing an error transformation to deal with the FoV constraints while ensuring prescribed control performance. Those works provide new insights into reliable, low-complexity FoV constraint controller design, and the robot control of the robot is considered at the dynamics level. Despite this, visual-robot coupled dynamics per se have not been dealt directly with the PPC algorithm.

In this work, we exploit an adaptive output feedback funnel control to address the FoV restrictions of the camera. Funnel control has been applied to constraint transient response of nonlinear systems [6, 24, 28, 41]. Yang et al. [41] utilizing a funnel function to guarantee the transient tracking performance of a robotic system with a predefined funnel boundary. In [6], a performance funnel function is employed to construct a fuzzy adaptive controller while ensuring the transient response. Barrier Lyapunov Function (BLF) has been proposed to design controllers for nonlinear systems in strict constraints form [21]. KP. Tee et al. [36] utilizes an asymmetric time-varying Barrier Lyapunov Function to achieve strict state constraints for nonlinear systems. Liu et. al [23] utilizing a funnel control scheme with a BLF to accomplish arbitrary output tracking accuracy of uncertain nonlinear system. The research [45] incorporated a constant symmetric BLF and a time-varying asymmetric BLF to deal with the visual system visibility problem. In [22], by using a log-type BLF to work out the steady landing problem of an IBVS-controlled quadrotor. In our previous works [14, 15], we employed a symmetric BLF to restrict visual features in the camera FoV. To the best of the author's knowledge, time-varying asymmetric BLF has not been implemented to handle the issue of image features escaping from the camera's FoV. Unlike the aforementioned research works, we present the FoV restriction for a visual servoing (VS) system with time-varying asymmetric BLF, where the state tracking error can converge to a predefined error bound ensuring a demanded transient response as well as required arbitrary error tracking precision.

Another critical issue is that the vision system is highly coupled with robot dynamics [11, 12]. Some research works ignore the robot dynamics in IBVS tasks, which is a feasible way to handle robots with slow motions [37]. To accommodate high-speed tasks, we propose a torque controller, but with unknown dynamics. Artificial neural networks have been confirmed to be able to approximate nonlinear functions with arbitrary accuracy under certain specific conditions [20]. Thus, artificial neural networks have been widely used in compensating uncertain dynamics of nonlinear systems [16, 47]. Adaptive fuzzy neural networks have excellent performance in approximating arbitrary nonlinear functions. Applying adaptive fuzzy neural networks for compensation of high-dimensional robot dynamics is a sensible choice, because of the simple parameterization and computational efficiency. For instance, Su et al. [35] introduced a decoupled adaptive fuzzy approximation technique with dynamical uncertainties in a teleoperated surgery scenario. Zhu et al. [48] developed a fixed-time fuzzy controller for robot manipulator dynamics. In [32], fuzzy neural networks are applied to design an adaptive controller to better the human-robot collaborative performance. Zhang et al. [42] proposed a fuzzy-neural controller for improving the collaborative control accuracy of multi-manipulator systems. In [46], an adaptive fuzzy prescribed performance algorithm is developed to estimate the unknown nonlinear dynamics of high-order nonlinear multiagent systems. In [40], adaptive fuzzy control is adopted to deal with the uncertain kinematics and dynamics that derive from strongly coupled nonlinearities of the dual-arm robot. Zhong et al. [30] designed an adaptive fuzzy control law for the strict-feedback nonlinear system to handle external disturbance. Thus, a fuzzy neural network (FNN) is employed in this work to compensate for the uncertain term in the torque controller, which is an intelligent choice since FNN requires only less information about the system dynamics. In summary,

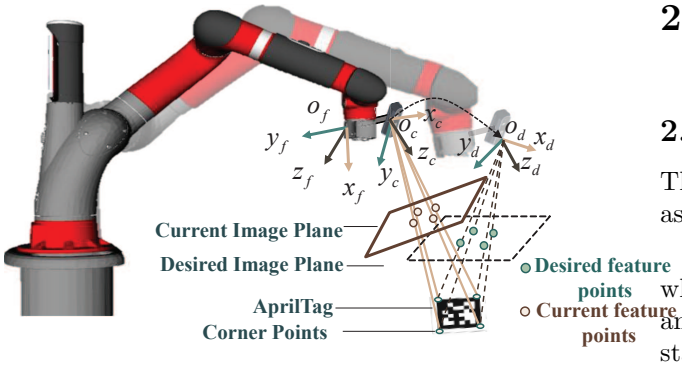

Figure 2: Schematic diagram of the operational mechanism of the vision servoing system.

the key contributions of our proposed control scheme compared to existing research work can be summarized as

1. A tunnel control scheme with a time-varying Barrier Lyapunov function is innovatively employed to design an IBVS constrained controller to restrain the feature points within the camera's field of view. The main contribution of the specified work is that the performance specification is a priori, designable, and imposed without increasing the complexity of the controller.

2. A time-varying BLF is implemented to ensure that the feature point tracking errors converge to a tightly specified range and to guarantee the transient response of tracking errors without requiring any a priori knowledge about the nonlinear visual servoing system. In contrast to our earlier work [15], we employed a time-varying BLF instead of a constant BLF to relax initial conditions of feature errors as well as customize any desired arbitrary tracking accuracy.

3. An adaptive controller is developed using fuzzy neural networks to compensate for uncertain dynamics. In particular, the high-coupling visual robot system affects the control performance. Thus, taking advantage of the adaptive torque controller contributes to better control accuracy of the IBVS task performance.

The rest of the paper is organized as follows. Section II introduces visual servoing system modeling, preliminaries, and problem statements. Section III presents the adaptive constrained IBVS controller and stability analysis. The experimental results are presented in section IV. Finally, section V concludes the paper.

2 Mathematical model and preliminaries

2.1 System Description

The system dynamics of an n-linked rigid robot stated as

$$M(q)\ddot{q} + C(q,\dot{q})\dot{q} + G(q) = \tau, \tag{1}$$

where $q, \dot{q}, \ddot{q} \in \Re^m$ represent the joint position, velocity, and acceleration state variables, respectively. $\tau \in \Re^m$ stands for the control signal, $M(q) \in \Re^{m\times m}$ is the symmetric positive definite inertia matrix, $C(q,\dot{q})\dot{q} \in \Re^m$ describes the Coriolis and centripetal forces matrix, and $G(q) \in \Re^m$ is the gravitational force vector.

To facilitate the subsequent derivation, we rewrite the above equality in the form of the state equation, as

$$\frac{d}{dt}\begin{bmatrix} q \\ \dot{q} \end{bmatrix} = \begin{bmatrix} \dot{q} \\ M^{-1}(q)[-C(q,\dot{q})\dot{q} - G(q) + \tau] \end{bmatrix}. \tag{2}$$

The end-effector velocity $V_e = [\upsilon_e \ \omega_e]^T$ which is related to the joint velocity $\dot{q}$ expressed in the end-effector frame, where υ_e and ω_e represent the translation and rotation velocity respectively, by

$$V_e = J_r(q)\dot{q}, \tag{3}$$

where $J_r(q) \in \Re^{6\times m}$ denotes the robot Jacobian.

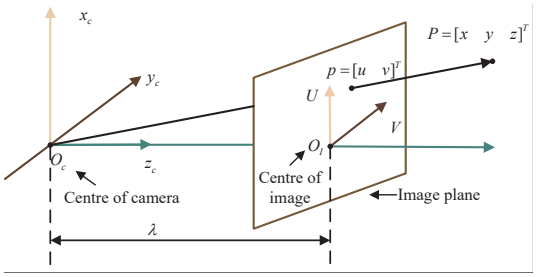

Figure 3: Universal pinhole camera geometry model.

Consider a visual servoing system in which the pinhole camera model is mounted at the robot end-effector, as shown in Fig.2. The geometric model of a pinhole camera is presented in Fig.3. The camera center O_c is linked to the camera frame C. O_I is the center of the pixel frame I, where z_c of the camera frame transverses O_I and perpendicular to the pixel plane. Given a group of 3D points $P_i = [x_i \ y_i \ z_i]^T, i = 1, ..., l$, we can obtain the respective 2D visual feature point $s_i = [u_i \ v_i]^T, i = 1, ..., l$, by

$$s_i = \begin{bmatrix} u_i \\ v_i \end{bmatrix} = \frac{\lambda}{z_i}\begin{bmatrix} x_i \\ y_i \end{bmatrix} \tag{4}$$

where λ denotes the focal length of the camera. The time differential of the image feature points is related to the spatial velocity V_c of the camera, we have

$$\dot{s}_i = L_i(z_i, s_i)V_c \tag{5}$$

where

$$L_i(z_i, s_i) = \begin{bmatrix} -\frac{\lambda}{z_i} & 0 & \frac{u_i}{z_i} & \frac{u_i v_i}{\lambda} & -\frac{\lambda^2+u_i^2}{\lambda} & v_i \\ 0 & -\frac{\lambda}{z_i} & \frac{v_i}{z_i} & \frac{\lambda^2+v_i^2}{\lambda} & -\frac{u_i v_i}{\lambda} & -u_i \end{bmatrix}$$

stands for the image interaction matrix, $V_c = [v_c\ w_c]^T$ is the spatial linear and angular velocity of the camera. Given the visual servoing system feature points vector $s = [s_1^T, ..., s_l^T]^T \in R^{2l}$. The dynamics of the vision system are described as

$$\dot{s} = L(z, s)V_c \tag{6}$$

and $L(z, s) = [L_1^T(z_1, u_1), L_1^T(z_1, v_1), ..., L_{2l}^T(z_l, v_l)]^T$ is the vision system interaction matrix and $z = [z_1, ..., z_l]^T$ is depth of the feature points.

To procedure the system dynamic modeling, we correlate the end-effector velocity of the robot manipulator with the camera's spatial velocity employing the velocity translation matrix W_{ce}, as

$$V_c = W_{ce}V_e \tag{7}$$

and W_{ce} is expressed as

$$W_{ce} = \begin{bmatrix} R_{ce} & [t_{ce}]_\times R_{ce} \\ 0_{3\times 3} & R_{[ce]} \end{bmatrix} \tag{8}$$

where $R_{ce} \in SO(3)$ is the rotation matrix, $t_{ce} \in \Re^3$ denotes the translation vector. $[t_{ce}]_\times$ represents the 3×3 skew-symmetric matrix. It's worth noting that W_{ce} is a constant matrix in this work, benefiting from the fact that the camera is rigidly mounted on the end-effector of the robot. Hence, combining (3), (5) and (7), the vision servo system dynamics are as follows

$$\dot{s} = J_s(z, s, q)\dot{q} \tag{9}$$

where $J_s = LW_{ce}J_r$ represents the task Jacobian.

Summarizing the above modeling process, we define a new state vector $Q = [s^T\ \dot{q}^T]^T \in \Re^{m+2l}$. Including (2) and (9), the visual servoing system dynamics is expressed as

$$\frac{d}{dt}\begin{bmatrix} s \\ \dot{q} \end{bmatrix} = \begin{bmatrix} J_s(z, s, q)\dot{q} \\ M^{-1}(q)[-C(q, \dot{q})\dot{q} - G(q) + \tau] \end{bmatrix}. \tag{10}$$

Define $x_1 = s,\ x_2 = \dot{q}$, we rewrite the system dynamics expression as

$$\begin{aligned} \dot{x}_1 &= J_s x_2 \\ \dot{x}_2 &= M^{-1}(q)[-C(q, \dot{q})\dot{q} - G(q) + \tau] \end{aligned} \tag{11}$$

where the feature point vector $x_1 = [x_{11}, x_{12}, ..., x_{1v}]^T \in R^v, v = 2l$. For limiting the image feature points to stay within the camera's FoV, the coordinates of the feature points are required to meet the following visibility restrictions

$$\chi_{min} \le \chi_i \le \chi_{max}, i = 1, 2, ..., 2l, \chi \in \{u, v\} \tag{12}$$

where χ_{min}, χ_{max} denote the lower and upper bounds of feature coordinates in pixels, respectively.

2.2 Fuzzy Neural Networks

Consider a fuzzy system consisting of N fuzzy IF-THEN rules, the form of linguistic rule is

$$\begin{aligned} &IF\ x_1\ is\ \zeta_1^k, ...\ and\ x_n\ is\ \zeta_n^k \\ &THEN,\ y\ is\ \xi^k,\ k = 1, ..., N. \end{aligned}$$

where $x = [x_1, ..., x_n]^T \in \Re^n$ and y are the linguistic variables with respect to the input and output of FNNs, respectively. $\zeta_i^k, i = 1, 2, ..., n$ and ξ^k are the fuzzy sets. The fuzzy neural network system is performed as follows

$$y(x) = \frac{\sum_{k=1}^N y_k \prod_{i=1}^n \mu_{\zeta_i^k}(x_i)}{\sum_{k=1}^N \Big(\prod_{i=1}^n \mu_{\zeta_i^k}(x_i)\Big)}. \tag{13}$$

where $\mu_{\zeta_i^k}(x_i)$ and $\mu_{\xi^k}(y)$ are the fuzzy membership functions, $y_k = max_{y\in\Re}\mu_{\xi^k}(y)$.

Define fuzzy basis function as

$$\varphi_k(x) = \frac{\Big(\prod_{i=1}^n \mu_{\zeta_i^k}(x_i)\Big)}{\sum_{k=1}^N \Big(\prod_{i=1}^n \mu_{\zeta_i^k}(x_i)\Big)}. \tag{14}$$

The weight vector and fuzzy basis function vector are defined as $\vartheta = [y_1, y_2, ..., y_N]^T$ and $\varphi(x) = [\varphi_1(x), \varphi_2(x), ..., \varphi_N(x)]^T$, respectively. Thus, equation 13 can be formulated as

$$y(x) = \vartheta^T\varphi(x). \tag{15}$$

The FNNs have excellent performance in approximating any continuous function $\Phi_i(x_i), i = 1, 2, ..., n$ with arbitrary accuracy on a compact set Ω.

2.3 Preliminaries

Lemma 1 [7]: For bounded initial conditions, if there exists a Lyapunov function $V(x)$ which is C^1 continuous and positive definite, satisfying $\kappa_1(\|x\|) \le V(x) \le \kappa_2(\|x\|)$, with $\dot{V}(x) \le -\rho V(x) + c$, where $\kappa_1, \kappa_2 : \Re^n \to \Re$ denote class κ functions, and ρ and c are two positive constants, yielding a solution $x(t)$ that is uniformly bounded.

Lemma 2 [31]: For any positive constant $|x| < 1$ and any any positive integer p, the following inequality holds:

$$\log\frac{1}{1 - x^{2p}} < \frac{x^{2p}}{1 - x^{2p}}$$

Property 1: The skew-symmetric matrix $\dot{M}(q) - 2C(q, \dot{q})$ meets the following equation

$$\dot{M}(q) - 2C(q, \dot{q}) = 0$$

2.4 Problem Statement

Consider a visual servoing system (10) in which a vision sensor attaches at the end-effector of an n-linked rigid robot manipulator, as shown in Fig.2. This work intends to design a constrained image-based controller, with the ability to tailor a priori and predetermined performance for image feature tracking errors, to constrain visual feature points continuously staying within the field of view of the camera. The visual features $s = [u\ v]^T$ will converge to a preset, small neighborhood around the desired constant visual feature s^*. Furthermore, all signals of the closed-loop system should remain bounded. The control strategy is presented in Fig.4

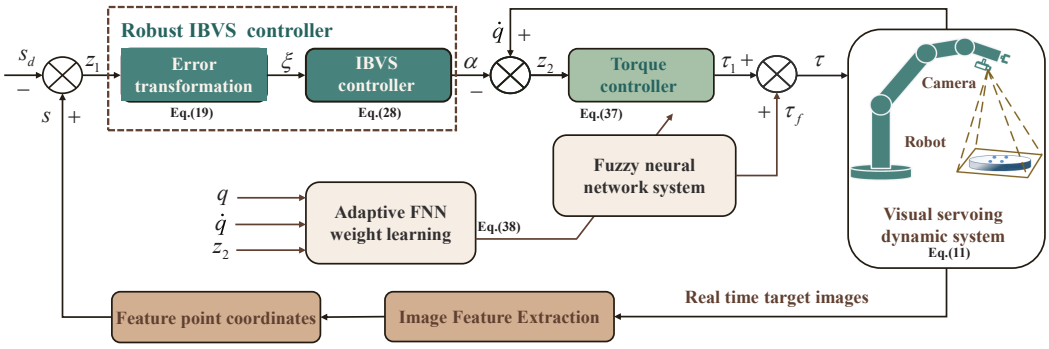

Figure 4: The control block diagram of the proposed algorithm in this paper.

3 Control design

To begin with, let us introduce the definition of the relevant tracking error signals:

$$\begin{aligned} z_1 &= x_1 - x_d, \\ z_2 &= x_2 - \alpha. \end{aligned} \tag{16}$$

where $z_1 = [z_{11}, z_{12}, ..., z_{1N}]^T \in \Re^N$, represent the image feature errors, $z_2 = [z_{21}, z_{22}, ..., z_{2M}]^T \in \Re^M$ stand for the joint velocity errors, and α is the virtual controller signal need to be specified later.

3.1 Performance Specification for Tracking Signals

To advance the controller design procedure, we import the concept of a performance tunnel $P_\rho(t)$ to shape the evolution of the tracking error $z_i, i = 1, 2, ..., N$, as follows:

$$P_\rho := \{(t, z_i) \in \Re_{\geq 0} \times \Re | \parallel z_i(t) \parallel < \rho_k(t)\}. \tag{17}$$

where $\Re_{\geq 0}$ represents a set of nonnegative real numbers.

It is worth noting that the funnel boundaries are flexible, thus, it's convenient to specify the error tracking performance, and in most situations, it is easy to choose a monotonic funnel. We define a funnel function $\rho_k(t), k = 1, 2, ..., N$ with an exponential decay form as:

$$\rho_k(t) = (\rho_k(0) - \rho_k^\infty)exp(-l_k t) + \rho_k^\infty. \tag{18}$$

where $l_k > 0, k = 1, 2, ..., N$ regulates the exponential convergence rate of the error, and $\rho_k(0) > 0$, $\rho_k^\infty > 0, k = 1, 2, ..., N$ are the maximum allowable error and the steady-state performance specification, respectively. They all need to be properly selected.

To perform error transformation, we define $\varphi_{a,k}(t) = -\beta_{1,k}\rho_k(t)$, $\varphi_{b,k}(t) = \beta_{2,k}\rho_k(t), k = 1, 2, ..., N$, where positive constant $\beta_{1,k}$ and $\beta_{2,k}$ are design parameters. The transferred error is performed as follows:

$$\begin{aligned} &\xi_a = \left[\frac{z_{11}}{\varphi_{a,1}}, ..., \frac{z_{1N}}{\varphi_{a,N}}\right]^T, \xi_b = \left[\frac{z_{11}}{\varphi_{b,1}}, ..., \frac{z_{1N}}{\varphi_{b,N}}\right]^T, \\ &\xi_k = q_k(z_{1k})\xi_{b,k} + (1 - q_k(z_{1k}))\xi_{a,k}. \end{aligned} \tag{19}$$

where $\xi_{a,k}$ and $\xi_{b,k}$ represent the kth element of the vectors ξ_a and ξ_b, respectively, and $q_k(z_{1k})$ is defied as

$$q_k(z_{1k}) := \begin{cases} 1 & z_{1k} > 0 \\ 0 & z_{1k} \leq 0. \end{cases}$$

3.2 Robust IBVS Controller Design

To guarantee the performance of the robot manipulator, an asymmetric time-varying barrier function is constructed as follows:

$$V_1 = \sum_{k=1}^{N}(\frac{q_k}{2}\ln\frac{1}{1-\xi_{b,k}^2} + \frac{1-q_k}{2}\ln\frac{1}{1-\xi_{a,k}^2}). \tag{20}$$

Derivative of (20) with respect to time, we have

$$\dot{V}_1 = \sum_{k=1}^{N}(\frac{q_k\xi_{b,k}\dot{\xi}_{b,k}}{1-\xi_{b,k}^2} + \frac{(1-q_k)\xi_{a,k}\dot{\xi}_{a,k}}{1-\xi_{a,k}^2}). \tag{21}$$

The differentiation of $\xi_{a,k}$ and $\xi_{b,k}$ with respect to time is given by

$$\begin{aligned} \dot{\xi}_{a,k} &= \frac{\dot{z}_{1k}}{\varphi_{a,k}} - \frac{z_{1k}\dot{\varphi}_{a,k}}{\varphi_{a,k}^2} \\ \dot{\xi}_{b,k} &= \frac{\dot{z}_{1k}}{\varphi_{b,k}} - \frac{z_{1k}\dot{\varphi}_{b,k}}{\varphi_{b,k}^2} \end{aligned} \tag{22}$$

Substituting (22) into (21), and exploiting error signals transformation formulation (19), we have

$$\begin{aligned} \dot{V}_1 &= \sum_{k=1}^{N}\left[\frac{q_k\xi_{b,k}^2}{(1-\xi_{b,k}^2)z_{1k}}(\dot{z}_{1k} - \frac{z_{1k}\dot{\varphi}_{b,k}}{\varphi_{b,k}})\right] \\ &+ \sum_{k=1}^{N}\left[\frac{(1-q_k)\xi_{a,k}^2}{(1-\xi_{a,k}^2)z_{1k}}(\dot{z}_{1k} - \frac{z_{1k}\dot{\varphi}_{a,k}}{\varphi_{a,k}})\right] \\ &= \sum_{k=1}^{N}\left[\frac{\xi_k^2\dot{z}_{1k}}{(1-\xi_k^2)z_{1k}} - \frac{q_k\xi_{b,k}^2}{1-\xi_{b,k}^2}\frac{\dot{\varphi}_{b,k}}{\varphi_{b,k}} - \frac{(1-q_k)\xi_{a,k}^2}{1-\xi_{a,k}^2}\frac{\dot{\varphi}_{a,k}}{\varphi_{a,k}}\right]. \end{aligned} \tag{23}$$

To facilitate the subsequent derivation, we define the transient variable

$$H = \left[\frac{\xi_1^2}{(1-\xi_1^2)z_{11}}, \frac{\xi_2^2}{(1-\xi_2^2)z_{12}}, ..., \frac{\xi_N^2}{(1-\xi_N^2)z_{1N}}\right]^T. \tag{24}$$

Thus, expression (23) is rewritten as

$$\dot{V}_1 = H^T \dot{z}_1 - \sum_{k=1}^{N} \left[\frac{q_k \xi_{b,k}^2}{(1-\xi_{b,k}^2)} \frac{\dot{\varphi}_{b,k}}{\varphi_{b,k}} + \frac{(1-q_k)\xi_{a,k}^2}{1-\xi_{a,k}^2} \frac{\dot{\varphi}_{a,k}}{\varphi_{a,k}} \right]. \tag{25}$$

According to the definition of error vectors, we obtain

$$\dot{z}_1 = J_s(z_2 + \alpha) - \dot{x}_d. \tag{26}$$

Thus, we have

$$\begin{aligned} \dot{V}_1 &= H^T(J_s(z_2+\alpha) - \dot{x}_d) \\ &\quad - \sum_{k=1}^{N} \left[\frac{q_k \xi_{b,k}^2}{(1-\xi_{b,k}^2)} \frac{\dot{\varphi}_{b,k}}{\varphi_{b,k}} + \frac{(1-q_k)\xi_{a,k}^2}{1-\xi_{a,k}^2} \frac{\dot{\varphi}_{a,k}}{\varphi_{a,k}} \right]. \end{aligned} \tag{27}$$

To ensure the nonlinear system Lyapunov stable, the stabilizing function is given by

$$\alpha = J_s^+ [\dot{x}_d - (k_1 + \bar{\sigma}(t)) z_1]. \tag{28}$$

where J_s^+ is the Moore-Penrose inverse of J_s, and $k_1 = diag(k_{11}, k_{12}, ..., k_{1N})$, the elements in k_1 are all positive constants. The time-varying gain $\bar{\sigma}$ is given by $\bar{\sigma}_k(t) = \sqrt{(\frac{\dot{\varphi}_{a,k}}{\varphi_{a,k}})^2 + (\frac{\dot{\varphi}_{b,k}}{\varphi_{b,k}})^2 + \omega}, k = 1, 2, ..., N$, where ω is any positive constant guarantees that the time derivative of α_k remains bounded even $\dot{\varphi}_{a,k}$ and $\dot{\varphi}_{b,k}$ are both zero. Substituting (28) into (27), yields

$$\begin{aligned} \dot{V}_1 &= H^T J_s z_2 - H^T (k_1 + \bar{\sigma}) z_1 \\ &\quad - \sum_{k=1}^{N} \left[\frac{q_k \xi_{b,k}^2}{1-\xi_{b,k}^2} \frac{\dot{\varphi}_{b,k}}{\varphi_{b,k}} + \frac{(1-q_k)\xi_{a,k}^2}{1-\xi_{a,k}^2} \frac{\dot{\varphi}_{a,k}}{\varphi_{a,k}} \right]. \end{aligned} \tag{29}$$

Noting that

$$\bar{\sigma}_k(t) + \frac{q_k \dot{\varphi}_{b,k}}{\varphi_{b,k}} + \frac{(1-q_k)\dot{\varphi}_{a,k}}{\varphi_{a,k}} \geq 0. \tag{30}$$

We obtain

$$\dot{V}_1 \leq \sum_{k=1}^{N} \left(-\frac{\xi_k^2}{1-\xi_k^2} k_{1k} \right) + H^T J_s z_2. \tag{31}$$

3.3 Adaptive Fuzzy NN Controller Design

Choose the Lyapunov candidate function

$$V_2 = V_1 + \frac{1}{2} z_2^T M z_2. \tag{32}$$

The time derivative of V_2 is given by

$$\dot{V}_2 = \dot{V}_1 + z_2^T M z_2 + \frac{1}{2} z_2^T \dot{M} z_2. \tag{33}$$

According to system dynamics expression (11) and the error definition (16), we can obtain

$$\begin{aligned} \dot{V}_2 &= \dot{V}_1 + z_2^T [-C(q,\dot{q})\alpha - G(q) - M(q)\dot{\alpha} + \tau] \\ &\quad + \frac{1}{2} z_2^T [\dot{M}(q) - 2C(q,\dot{q})] z_2. \end{aligned} \tag{34}$$

Referring to the literature [33], the term $\dot{M}(q) - 2C(q,\dot{q})$ is equal to zero, thus

$$\dot{V}_2 = \dot{V}_1 + z_2^T [-C(q,\dot{q})\alpha - G(q) - M(q)\dot{\alpha} + \tau]. \tag{35}$$

Using FNNs to approximate the unknown part $-C(q,\dot{q})\alpha - G(q) - M(q)\dot{\alpha}$ with arbitrary accuracy, define

$$F(Z) = -C(q,\dot{q})\alpha - G(q) - M(q)\dot{\alpha}. \tag{36}$$

where $F(Z) = [s_1(Z), s_2(Z), ..., s_{N_0}(Z)]^T$, $Z = [q^T, \dot{q}^T, \alpha^T, \dot{\alpha}^T]^T \in \Re^p$, with $p = 4N_0$. We define $F(Z) = \theta^{*T}\phi(Z)$, where $\theta^* = [\theta_1^*, \theta_2^*, ..., \theta_M^*]^T$ and $\phi(Z) = [\phi_1(Z), \phi_2(Z), ..., \phi_M(Z)]^T$. Combined with the adaptive fuzzy neural network, we propose the following controller

$$\tau = -k_2 z_2 - \hat{F}(Z) - H^T J_s. \tag{37}$$

where $k_2 = diag(k_{21}, k_{22}, ..., k_{2M})$ with k_{2k} represents the kth element in k_2, $\hat{F}(Z) = \hat{\theta}^T \phi(Z) + \varepsilon$ with the estimation error satisfying $|\varepsilon| < \delta$, δ is any positive constant.

The fuzzy neural network weight adaptive law is designed as

$$\dot{\hat{\theta}}_k = \Gamma_k (z_{2k} \phi(Z_k) - \gamma_k \hat{\theta}_k). \tag{38}$$

where Γ_k and $\gamma_k, k = 1, 2, ..., M$ denote positive constants.

To confirm the proposed controller Lyapunov stability, we choose the candidate as

$$V = V_2 + \frac{1}{2} \sum_{k=1}^{M} \tilde{\theta}_k^T \Gamma_k^- 1 \tilde{\theta}_k. \tag{39}$$

where $\tilde{(*)} = \hat{(*)} - (*)$. Differentiating V with respect to time, considering the control law in (37), yields

$$\begin{aligned} \dot{V} &\leq z_2^T (\theta^{*T}\phi(Z) - \hat{\theta}^T \phi(Z) - \varepsilon - H^T J_s - k_2 z_2) \\ &\quad + H^T J_s z_2 - \sum_{k=1}^{N} \frac{\xi_k^2}{1-\xi_k^2} k_{1k} + \sum_{k=1}^{M} \tilde{\theta}_k^T \Gamma_k^- 1 \dot{\hat{\theta}}_k. \end{aligned} \tag{40}$$

Taking the adaptive update law (38) in consideration, obtain

$$\dot{V} \leq -z_2^T k_2 z_2 - z_2^T \varepsilon + \sum_{k=1}^{M} \tilde{\theta}_k^T \gamma_k (\tilde{\theta}_k + \theta_k^*) - \sum_{k=1}^{N} \frac{\xi_k^2}{1-\xi_k^2} k_{1k}. \tag{41}$$

Taking full advantage of Young's inequality, we have

$$-z_2^T \varepsilon \leq \frac{1}{2} \|z_2\|^2 + \frac{1}{2} \varepsilon^2 \tag{42}$$

$$-\sum_{k=1}^{M} \tilde{\theta}_k^T \gamma_k (\tilde{\theta}_k + \theta_k^*) \leq -\sum_{k=1}^{M} \frac{\gamma_k}{2} \tilde{\theta}_k^T \tilde{\theta}_k + \sum_{k=1}^{M} \frac{\gamma_k}{2} \theta_k^{*T} \theta_k^* \tag{43}$$

Substituting (42)-(43) in to (41), and exploiting Lemma 2, we have

$$\begin{aligned}\dot{V} \leq & -z_2^T k_2 z_2 + \frac{1}{2}\|z_2\|^2 + \frac{1}{2}\varepsilon^2 - \sum_{k=1}^{N}\frac{\xi_k^2}{1-\xi_k^2}k_{1k} \\ & - \sum_{k=1}^{M}\frac{\gamma_k}{2}\tilde{\theta}_k^T\tilde{\theta}_k + \sum_{k=1}^{M}\frac{\gamma_k}{2}\theta_k^{*T}\theta_k^* \\ & \leq -\sum_{k=1}^{N}k_{1k}\ln\frac{1}{1-\xi_k^2} - \frac{2k_2-1}{M}(\frac{1}{2}z_2^T M z_2) \\ & - \frac{\gamma}{\Gamma^{-1}}(\frac{1}{2}\tilde{\theta}^T\Gamma^{-1}\tilde{\theta}) + \frac{1}{2}\varepsilon^2 + \frac{\gamma}{2}\|\theta^*\|^2.\end{aligned} \tag{44}$$

3.4 Stability Analysis

Theorem 1. *For the visual servoing system in* (11)*, the robust IBVS controller in* (28)*, the adaptive controller in* (37)*, the FNN weights adaptive update law* (38)*, and the performance specification function* (18)*. Given initial condition that* $z_{1k}(0)$ *satisfies* $\varphi_{a,k}(0) < z_{1k}(0) < \varphi_{b,k}(0)$*. The performance of the visual servoing system can be concluded as*

(1) The tracking signals z_1*,* z_2*,* $\tilde{\theta}$ *of the closed loop system are uniformly ultimately bounded.*

(2) The tracking error vector z_1 *is constrained to the boundaries of the performance specified function.*

(3) The tracking error z_1 *will converge into a small region nearby zero.*

Proof. By the previous derivation, the final formulation of the Lyapunov function V is

$$V = \frac{1}{2}\sum_{k=1}^{N}\ln\frac{1}{1-\xi_k^2} + \frac{1}{2}z_2^T M z_2 + \frac{1}{2}\tilde{\theta}^T\Gamma^{-1}\tilde{\theta}. \tag{45}$$

The inequality (44) can be formulated as

$$\dot{V} \leq -aV + b. \tag{46}$$

where $a = min\{2\lambda_{min}(k_1), \frac{2\lambda_{min}(k_2)-1}{\lambda_{max}(M)}, \frac{\lambda_{min}\gamma}{\lambda_{max}\Gamma^{-1}}\}$, $b = \frac{1}{2}\varepsilon^2 + \frac{\gamma}{2}\|\theta^*\|^2$, $\lambda_{min}(*)$ and $\lambda_{max}(*)$ represent minimum and maximum eigenvalues of matrix $(*)$, respectively.

By further solve inequality (46), it given us that $V \leq V(0) + b/a$. Also considering the initial condition $\xi_k(0)$, we can deduce that the term of $\ln\frac{1}{1-\xi_k^2}$, the auxiliary error z_2, and the adaptive FNN weight error $\tilde{\theta}$ is bounded. Thus, we can surmise that $\varphi_a < z_1 < \varphi_b$ and the transient performance of control errors is guaranteed. Since φ_a and φ_b are limited functions, implies that z_1 is bounded. From the definition of error signals, x must be bounded, and in light of the formulation of (28), α is bounded as J_s is limited. Therefore, we can smoothly conclude that x_2 is bounded because $x_2 = z_2 + \alpha$. Ultimately, we prove that all signals are bounded. □

4 Experimental

In this portion, the theoretical results are verified by practical experiments. The validation platform consists of the Sawyer robot, a 7-DoF redundant robot manipulator, with a RealSense D435i camera mounted on the end-effector, as shown in Fig.2. The Sawyer robot is actuated by a built-in Intera SDK, and the host computer is equipped with Ubuntu 18.04. The FNN system and weight learning laws are training on a slave machine and communication with the host for the torque compensation in the form of ROS topic. To quickly verify the effectiveness of the algorithm and reduce the experimental procedure, we use the AprilTag cooperating with the Visual Servoing Platform (ViSP) [26] extracting corner points as visual features. The control signals of the Sawyer run at a frequency of about 500 Hz, and feature points are refreshed at roughly 35 Hz.

To clarify the validity and the robustness of the proposed method, two sets of comparative experiments were conducted as follows:

Case 1: Point-to-point tracking experiment. A set of visual feature points moves to a set of desired feature points.

Case 2: Large-amplitude cycle following experiment. A set of visual feature points rotation 45 degrees to a set of desired feature points.

We utilize a classical VS control law and a Proportion Integration Differentiation (PID) controller as a comparison to elucidate the effectiveness of the above two sets of experiments with the following expressions:

$$\begin{aligned}v_c = & -\lambda L^+(x_1 - x_d), \\ \tau_c = & -K_P(q(t) - q_d(t)) - K_D(x_2(t) - \alpha(t)) \\ & + K_I\int(q(t) - q_d(t))dt.\end{aligned}$$

Remark: In the experimental section we conducted two sets of experiments, the purpose of which is that, in comparison to the point-to-point tracking experiment, the rotational experiment under torque control has a larger motion and increased probability that the trajectories exceed the FoV, so we conducted a set of comparative experiments of point-to-point tracking to illustrate the effectiveness of the proposed algorithm. The rotation comparative experiments are conducted to illustrate the superior performance of the proposed algorithm.

To ease the progression of the experiments, we control in image coordinates rather than pixel coordinates because the error increases by a multiple in the pixel coordinate plane, so a small deviation in the coordinates of the feature points projected to the actual system will bring about a large error, leading to a deterioration in the control performance, which may further amplify the error and cause the system to be unstable.

For the fuzzy neural networks, choose Gaussian kernel functions as the affiliation function, which are continuously differentiable and advantageous in the theoretical analysis of FNN. For the Sawyer robot,

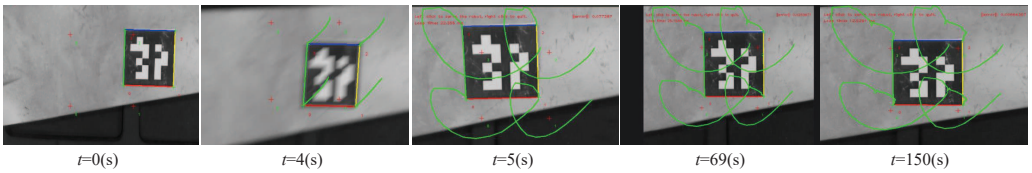

(a)

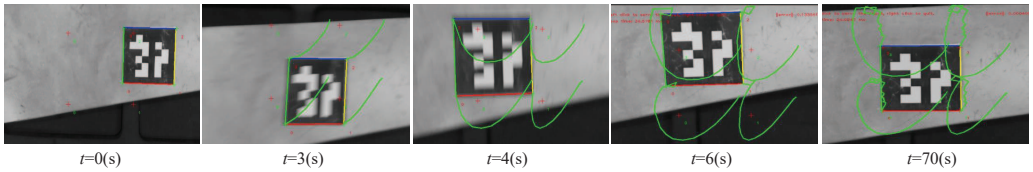

(b)

Figure 5: *Case 1:* Point-to-point tracking experiment. Motion trajectories of four image feature points in the actual FoV of the camera. (a) Classical IBVS controller. (b) Our proposed controllers. (Green cross: current image feature points; red cross: desired image feature points.)

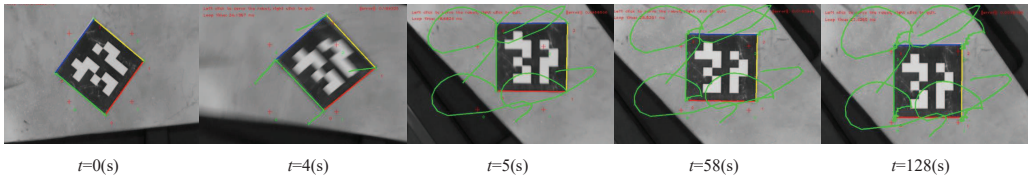

(a)

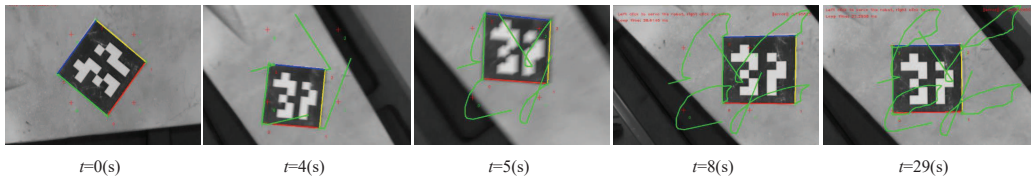

(b)

Figure 6: *Case 2:* Large-amplitude cycle following experiment. Motion trajectories of four image feature points in the actual FoV of the camera. (a) Classical IBVS controller. (b) Our proposed controllers. (Green cross: current image feature points; red cross: desired image feature points.)

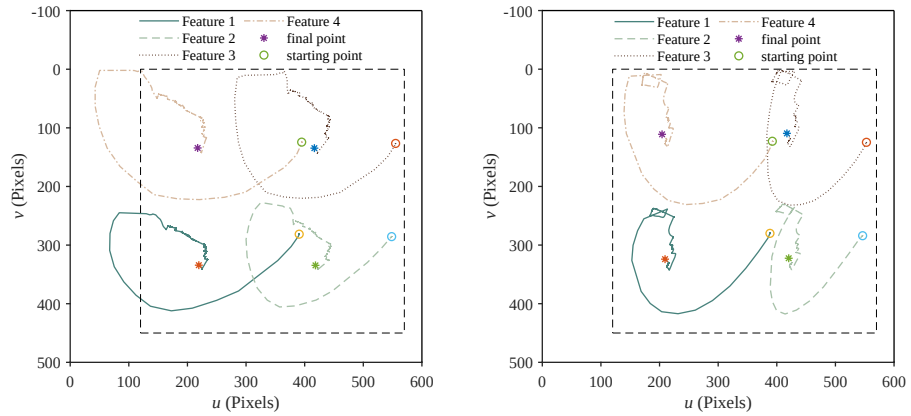

(a) (b)

Figure 7: *Case 1:* Point-to-point tracking experiment. Motion trajectories of four image feature points in the pixel plane. (a) Classical IBVS controller. (b) Our proposed controllers. The dotted rectangle represents the camera's FoV that we preset, which $u_{max} = 570$ (pixels), $v_{max} = 450$ (pixels), $u_{min} = 120$ (pixels), $v_{min} = 0$ (pixels).

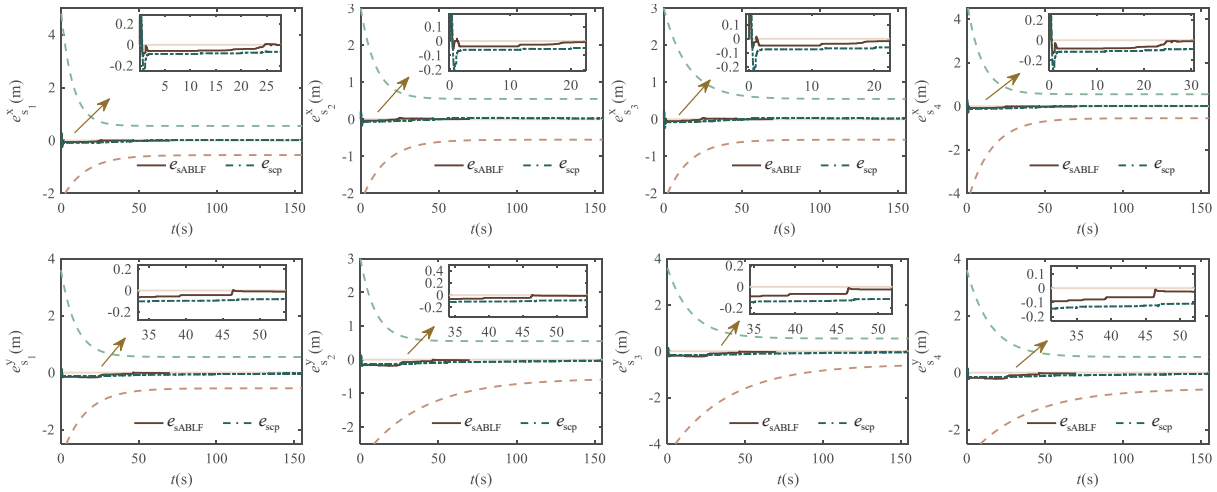

Figure 8: *Case 1:* Point-to-point tracking experiment. The evolution of the image feature errors along with the corresponding funnel boundaries (Green dashed decay line: funnel upper bound, brown dashed rise line: funnel lower bound).

each variable has 7 inputs since it is a 7-DoF redundant robot. Thus, to improve the FNN efficiency of training, we choose $[q^T, \dot{q}^T]^T \in R^{2M}$ as input variables. We set two central points for each input variable, leading to $p = 2^{2\times7} = 16384$ fuzzy rules. For case 1, the central points of the FNN are select from the area $[-0.05, 0.05] \times [-0.1, 0.1] \times [-0.05, 0.05] \times [-0.05, 0.05] \times [-0.05, 0.05] \times [-0.15, 0.05] \times [-0.1, 0.05] \times [-0.1, 0.1] \times [-0.1, 0.1] \times [-0.1, 0.1] \times [-0.1, 0.1] \times [-0.1, 0.1] \times [-0.1, 0.1]$, and the standard deviations for the FNN is $b_1 = [0.12, 0.24, 0.12, 0.12, 0.12, 0.24, 0.18, 0.24, 0.24, 0.24, 0.24, 0.24, 0.24, 0.24]^T$. For case 2, the central points of the FNN are select from the area $[-1.2, -0.8] \times [-1, -0.8] \times [0.2, 0.8] \times [1.8, 2.2] \times [-0.6, -0.2] \times [0.2, 0.8] \times [-0.9, 0.1] \times [-0.5, 0.5] \times [-0.5, 0.5] \times [-0.5, 0.5] \times [-0.5, 0.5] \times [-0.5, 0.5] \times [-0.5, 0.5]$, and the standard deviations for the FNN is $b_2 = [0.48, 0.24, 0.72, 0.48, 0.48, 0.72, 1.2, 1.2, 1.2, 1.2, 1.2, 1.2, 1.2, 1.2]^T$. The initial weights are preset to be $\hat{\theta}(0) = 0$. The adaptive gains of the weights learning law (38) is $\Gamma = 10$, $\gamma = 0.002$.

Remark: For the fuzzy neural network training segment, we retrain the FNN parameters by collecting data on joint angles q and joint angular velocities $\dot{q}$ prospectively. The retrained FNN parameters are reused in the later experiment. Since the visual servoing task converges from one set of points to another in a very short period, there is not enough time for FNN to do online training.

4.1 Point to Point Tracking Experiment

In this case, the initial coordinates of feature points in pixels are $s_{init} = [388, 280, 546, 284, 552, 124, 392, 122]^T(Pixels)$, and the desired feature points were preset as $s^* = [209, 324, 420, 322, 417, 109, 204, 111]^T(Pixels)$. For the comparison experimental group, the parameter of v_c is chosen as $\lambda = 0.5$, and parameters of τ_c are $K_P = diag(100, 80, 50, 40, 36, 26, 6)$, $K_D = diag(10.0, 6.0, 5.0, 3.0, 2.6, 1.9, 0.5)$, $K_I = diag(15, 8, 10, 10, 5, 4, 1)$. The parameters of funnel functions were set as $\rho_a(0) = [2.25, 3.0, 2.25, 3.0, 2.25, 4.5, 4.5, 3.0]^T$, $\rho_b(0) = [4.8, 3.6, 3.0, 3.0, 3.0, 3.6, 4.8, 3.6]^T$, $\rho^\infty_{a,k} = \rho^\infty_{b,k} = 0.55$ for $k = 1, ..., 8$, $l_a = [0.05, 0.05, 0.05, 0.02, 0.05, 0.02, 0.05, 0.02]^T$ and $l_b = [0.1, 0.08, 0.08, 0.08, 0.05, 0.05, 0.08, 0.05]^T$. Fig.5 shows the trajectories of the four image feature points observed in the camera's FoV converging from the current feature points (green crosses) to the desired feature points (red crosses). Fig.5(a) shows the trajectories of the feature points under classical visual servoing control, and Fig.5(b) shows the trajectories of the feature points under the constraints of the funnel function. It is noticeable that the range covered by the image feature point trajectories of our proposed controller is markedly smaller than that of the classical visual servoing controller. To emphasize the effectiveness of the FoV constraint algorithm, we plot the trajectories in the pixel coordinate system, as shown in Fig.7. The dotted boxes were the preset FoV. In Fig.7(a), the features 3 and 4 run out of the boxes, VS task failed. Introducing the funnel constraints, the features are well restricted to the FoV, as depicted in Fig.7(b). Fig.8 demonstrated the feature errors convergence curves, as can be seen in the detailed zoomed-in plot, the error values under the funnel function are noticeably reduced, and the convergence time of the tracking error is noticeably shorter, which saves about $80(s)$ compared to the classical vision servoing (i.e., $t_{ABLF} = 70(s)$ and $t_{cp} = 150(s)$). We utilize pre-trained FNN compensating the uncertain dynamics of the Sawyer robot, the weights of FNN were converged as indicated in Fig.11(a). Seen Fig.7(b), the final stage trajectories of the feature

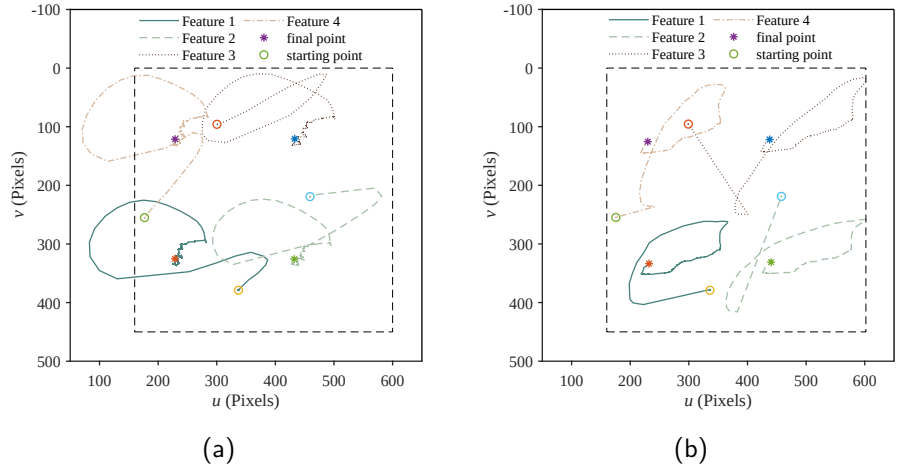

Figure 9: *Case 2:* Large-amplitude cycle following experiment. Motion trajectories of four image feature points in the pixel plane. (a) Classical IBVS controller. (b) Our proposed controllers. The dotted rectangle represents the camera's FoV that we preset, which $u_{max} = 600$ (pixels), $v_{max} = 450$ (pixels), $u_{min} = 160$ (pixels), $v_{min} = 0$ (pixels).

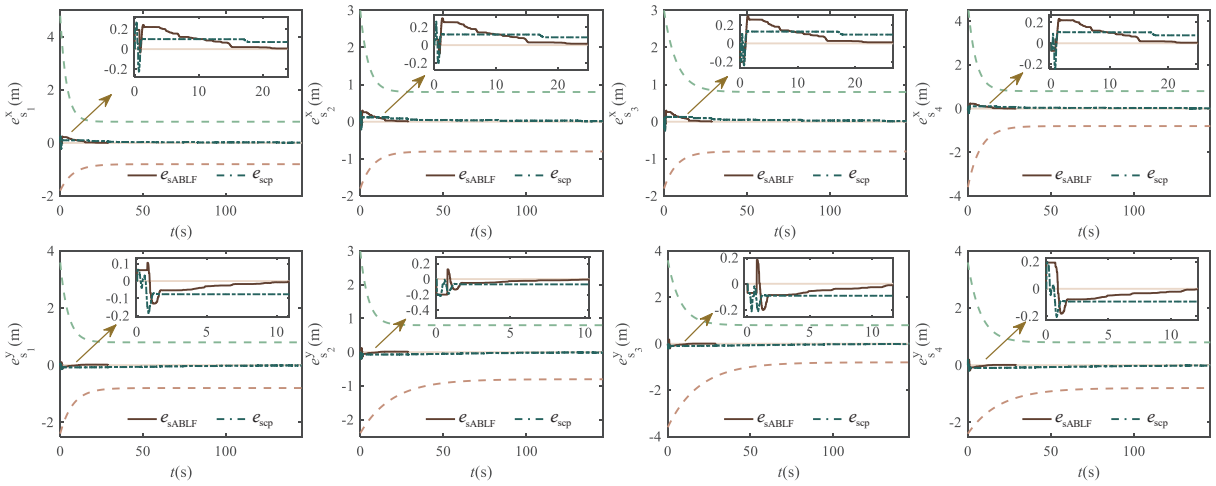

Figure 10: *Case 2:* Large-amplitude cycle following experiment. The evolution of the image feature errors along with the corresponding funnel boundaries (Green dashed decay line: funnel upper bound, brown dashed rise line: funnel lower bound).

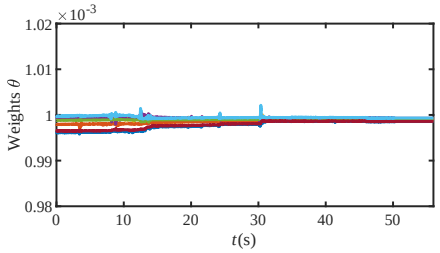

(a)

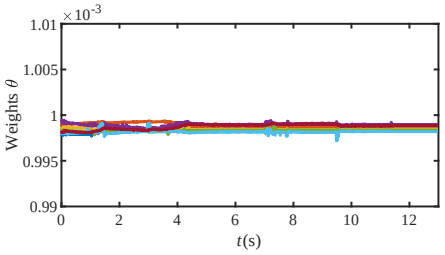

(b)

Figure 11: FNN weights θ. (a) Convergent weights in point-to-point tracking experiments. (b) Convergent weights in large-amplitude cycle following experiment.

points near the desired targets are smoother.

4.2 Large-amplitude Cycle Following Experiment

We implemented a set of rotational experiments to further illustrate the superior performance of the presented algorithm. In case 2, the initial feature points are $s_{init} = [335, 378, 457, 218, 299, 95, 175, 254]^T(Pixels)$, the desired image features are preset as $s^* = [219, 339, 421, 339, 421, 138, 219, 138]^T(Pixels)$. For the comparison experiment parameters, $\lambda = 0.5$, and $K_P = diag(60, 80, 30, 30, 36, 26, 6)$, $K_D = diag(6.0, 6.0, 3.0, 3.0, 2.6, 1.9, 0.5)$, $K_I = diag(8, 8, 6, 5, 5, 4, 1)$. The arguments to the funnel performance function are set to $\rho_a(0) = [1.5, 2.0, 1.5, 2.0, 1.5, 3.0, 3.0, 2.0]^T$, $\rho_b(0) = [4.0, 3.0, 2.5, 2.5, 2.5, 3.0, 4.0, 3.0]^T$, $\rho^{\infty}_{a,k} = \rho^{\infty}_{b,k} = 0.8$ for $k = 1, 2, ..., 8$, $l_a = [0.1, 0.1, 0.1, 0.04, 0.1, 0.04, 0.1, 0.04]^T$ and $l_b = [0.2, 0.16, 0.16, 0.16, 0.1, 0.1, 0.16, 0.1]^T$.

Fig.6 shows the trajectories of the current image features converge to desired ones with rotation 45 degrees. Fig.6(a) illustrates the trajectories without constraints. Fig.6(b) records the trajectories of feature points within the FoV of the camera with the funnel performance function constraints. Similarly, we draw the trajectories in the pixel plane as shown in Fig.9. It can be obviously observed from Fig.9(a) that features 3 and 4 escape from our preset range of FoV, while all image features are confined to the pre-defined FoV as shown in Fig.9(b). Fig.10 indicates the feature errors convergent trajectories. The feature errors derived from the constrained controller produce lower values than errors generated by the unconstrained controller, and e_{sABLF} converging at around $t_{ABLF} = 29(s)$, while e_{scp} takes about $128(s)$ approaching zero. By applying FNN in the torque controller, comparing the approaching stage to desired features, Fig.9(b) has smoother trajectories. Fig.11(b) demonstrates converged FNN weights.

5 Conclusion

In this paper, a robust IBVS controller was designed by introducing a funnel function to customize the performance of VS tasks, while respecting the camera's FoV. A time-varying BLF was implemented to specify the transient response of the VS system and ensure system stability. A torque controller was applied to accommodate high-speed robot motion and introduced a fuzzy neural network to compensate for the highly coupled vision-robot system dynamics. The proposed controllers were low complexity and require no a priori knowledge of the VS system. Experiment results have substantiated the effectiveness of the proposed controller.

Nevertheless, our proposed method exhibits some limitations. Theoretically, the proposed method can only guarantee that the tracking error converges to a neighborhood close to zero, but not to an arbitrarily small region. Meanwhile, the fuzzy neural network is collecting data for offline training and then reusing the parameters for online compensation, and the online update algorithm can be considered in the future. In addition, future industrial robots will require more intelligence and flexibility. We are considering introducing force perception combined with a vision for more complex tasks.

References

[1] Akbar Assa and Farrokh Janabi-Sharifi. Robust model predictive control for visual servoing. In *Proc. IEEE/RSJ Int. Conf. Intell. Robot. Syst.*, pages 2715–2720, 2014.

[2] Charalampos P. Bechlioulis, Shahab Heshmati-alamdari, George C. Karras, and Kostas J. Kyriakopoulos. Robust image-based visual servoing with prescribed performance under field of view constraints. *IEEE Trans. Rob.*, 35(4):1063–1070, 2019.

[3] Francois Chaumette and Seth Hutchinson. Visual servo control. i. basic approaches. *IEEE Robot. Autom. Mag.*, 13(4):82–90, 2006.

[4] Zhiwei Cui, Weibing Li, Xue Zhang, Philip Wai Yan Chiu, and Zheng Li. Accelerated dual neural network controller for visual servoing of flexible endoscopic robot with tracking error, joint motion, and rcm constraints. *IEEE Trans. Ind. Electron.*, 69(9):9246–9257, 2022.

[5] N. Garcia-Aracil, E. Malis, R. Aracil-Santonja, and C. Perez-Vidal. Continuous visual servoing despite the changes of visibility in image features. *IEEE Trans. Rob.*, 21(6):1214–1220, 2005.

[6] Xiyue Guo, Huaguang Zhang, Jiayue Sun, and Yu Zhou. Fixed-time fuzzy adaptive control of manipulator systems under multiple constraints: A modified dynamic surface control approach. *IEEE Trans. Syst. Man Cybern. Syst.*, 53(4):2522–2532, 2023.

[7] Wei He, Shuzhi Sam Ge, Bernard Voon Ee How, and Yoo Sang Choo. *Dynamics and control of mechanical systems in offshore engineering*. London, U.K.: Springer-Verlag, 2014.

[8] Shahab Heshmati-alamdari, Charalampos P. Bechlioulis, Minas V. Liarokapis, and Kostas J. Kyriakopoulos. Prescribed performance image based visual servoing under field of view constraints. In *Proc. IEEE/RSJ Int. Conf. Intell. Robot. Syst.*, pages 2721–2726, 2014.

[9] Shahab Heshmati-alamdari, George K. Karavas, Alina Eqtami, Michael Drossakis, and Kostas J. Kyriakopoulos. Robustness analysis of model predictive control for constrained image-based visual servoing. In *Proc. IEEE Int. Conf. Robot. Automat.*, pages 4469–4474, 2014.

[10] Shahab Heshmati-alamdari, George C. Karras, Alina Eqtami, and Kostas J. Kyriakopoulos. A robust self triggered image based visual servoing model predictive control scheme for small autonomous robots. In *Proc. IEEE/RSJ Int. Conf. Intell. Robot. Syst.*, pages 5492–5497, 2015.

[11] Yingbai Hu, Guang Chen, Zhijun Li, and Alois Knoll. Robot policy improvement with natural evolution strategies for stable nonlinear dynamical system. *IEEE Trans. Cybern.*, 53(6):4002–4014, 2023.

[12] Yingbai Hu, Zhijun Li, and Gary G. Yen. A knee-guided evolutionary computation design for motor performance limitations of a class of robot with strong nonlinear dynamic coupling. *IEEE Trans. Syst. Man Cybern. Syst.*, 53(7):4429–4441, 2023.

[13] Yanting Huang, Ming Zhu, Zewei Zheng, and Kin Huat Low. Linear velocity-free visual servoing control for unmanned helicopter landing on a ship with visibility constraint. *IEEE Trans. Syst. Man Cybern. Syst.*, 52(5):2979–2993, 2022.

[14] Jiao Jiang, Yaonan Wang, Yiming Jiang, and Zhiqiang Miao. Adaptive nn based visual servoing control for robot manipulator with field of view constraints and dynamic uncertainties. In *Proc. IEEE Int. Conf. Robot. Biomimetics*, pages 1694–1699, 2021.

[15] Jiao Jiang, Yaonan Wang, Yiming Jiang, He Xie, Haoran Tan, and Hui Zhang. A robust visual servoing controller for anthropomorphic manipulators with field-of-view constraints and swivel-angle motion: Overcoming system uncertainty and improving control performance. *IEEE Robot. Autom. Mag.*, 29(4):104–114, 2022.

[16] Yiming Jiang, Yaonan Wang, Zhiqiang Miao, Jing Na, Zhijia Zhao, and Chenguang Yang. Composite-learning-based adaptive neural control for dual-arm robots with relative motion. *IEEE Trans. Neural Netw. Learn. Syst.*, 33(3):1010–1021, 2022.

[17] Zhehao Jin, Jinhui Wu, Andong Liu, Wen-An Zhang, and Li Yu. Policy-based deep reinforcement learning for visual servoing control of mobile robots with visibility constraints. *IEEE Trans. Ind. Electron.*, 69(2):1898–1908, 2022.

[18] Moslem Kazemi, Kamal K. Gupta, and Mehran Mehrandezh. Randomized kinodynamic planning for robust visual servoing. *IEEE Trans. Rob.*, 29(5):1197–1211, 2013.

[19] Mohammad Keshmiri and Wen-Fang Xie. Image-based visual servoing using an optimized trajectory planning technique. *IEEE/ASME Trans. Mechatron.*, 22(1):359–370, 2017.

[20] A.U. Levin and K.S. Narendra. Control of nonlinear dynamical systems using neural networks. ii. observability, identification, and control. *IEEE Trans. Neural Networks*, 7(1):30–42, 1996.

[21] Zhijun Li, Guoxin Li, Xiaoyu Wu, Zhen Kan, Hang Su, and Yueyue Liu. Asymmetric cooperation control of dual-arm exoskeletons using human collaborative manipulation models. *IEEE Trans. Cybern.*, 52(11):12126–12139, 2022.

[22] Jie Lin, Yaonan Wang, Zhiqiang Miao, Hesheng Wang, and Rafael Fierro. Robust image-based landing control of a quadrotor on an unpredictable moving vehicle using circle features. *IEEE Trans. Autom. Sci. Eng.*, 20(2):1429–1440, 2023.

[23] Yong-Hua Liu, Chun-Yi Su, and Hongyi Li. Adaptive output feedback funnel control of uncertain nonlinear systems with arbitrary relative degree. *IEEE Trans. Autom. Control*, 66(6):2854–2860, 2021.

[24] Yong-Hua Liu, Chun-Yi Su, and Qi Zhou. Funnel control of uncertain high-order nonlinear systems with unknown rational powers. *IEEE Trans. Syst. Man Cybern. Syst.*, 51(9):5732–5741, 2021.

[25] E. Malis, F. Chaumette, and S. Boudet. 2 1/2 d visual servoing. *IEEE Trans. Robot. Automat.*, 15(2):238–250, 1999.

[26] E. Marchand, F. Spindler, and F. Chaumette. Visp for visual servoing: a generic software platform with a wide class of robot control skills. *IEEE Robot. Autom. Mag.*, 12(4):40–52, 2005.

[27] Zhiqiang Miao, Hang Zhong, Yaonan Wang, Hui Zhang, Haoran Tan, and Rafael Fierro. Low-complexity leader-following formation control of mobile robots using only fov-constrained visual feedback. *IEEE Trans. Ind. Inform.*, 18(7):4665–4673, 2022.

[28] Xiao Min, Simone Baldi, and Wenwu Yu. Distributed output feedback funnel control for uncertain nonlinear multiagent systems. *IEEE Trans. Fuzzy Syst.*, 30(9):3708–3721, 2022.

[29] Ravi Prakash and Laxmidhar Behera. Neural optimal control for constrained visual servoing via learning from demonstration. *IEEE Trans. Autom. Sci. Eng.*, pages 1–14, 2023.

[30] Jianbin Qiu, Tong Wang, Kangkang Sun, Imre J. Rudas, and Huijun Gao. Disturbance observer-based adaptive fuzzy control for strict-feedback nonlinear systems with finite-time prescribed performance. *IEEE Trans. Fuzzy Syst.*, 30(4):1175–1184, 2022.

[31] Beibei Ren, Shuzhi Sam Ge, Keng Peng Tee, and Tong Heng Lee. Adaptive neural control for output feedback nonlinear systems using a barrier lyapunov function. *IEEE Trans. Neural Networks*, 21(8):1339–1345, 2010.

[32] Xiaoqian Ren, Zhijun Li, MengChu Zhou, and Yingbai Hu. Human intention-aware motion planning and adaptive fuzzy control for a collaborative robot with flexible joints. *IEEE Trans. Fuzzy Syst.*, 31(7):2375–2388, 2023.

[33] Tong Heng Lee Sam Shuzhi Ge and Christopher J Harris. *Adaptive neural network control of robotic manipulators*. Singapore: World Scientific, 1998.

[34] Haobin Shi, Meng Xu, and Kao-Shing Hwang. A fuzzy adaptive approach to decoupled visual servoing for a wheeled mobile robot. *IEEE Trans. Fuzzy Syst.*, 28(12):3229–3243, 2020.

[35] Hang Su, Wen Qi, Jiahao Chen, and Dandan Zhang. Fuzzy approximation-based task-space control of robot manipulators with remote center of motion constraint. *IEEE Trans. Fuzzy Syst.*, 30(6):1564–1573, 2022.

[36] Keng Peng Tee, Beibei Ren, and Shuzhi Sam Ge. Control of nonlinear systems with time-varying output constraints. *Automatica J. IFAC*, 47(11):2511–2516, 2011.

[37] Pavlos D. Triantafyllou, George A. Rovithakis, and Zoe Doulgeri. Constrained visual servoing under uncertain dynamics. *Int. J. Control*, 92(9):2099–2111, 2019.

[38] Runhua Wang, Xuebo Zhang, Yongchun Fang, and Baoquan Li. Virtual-goal-guided rrt for visual servoing of mobile robots with fov constraint. *IEEE Trans. Syst. Man Cybern. Syst.*, 52(4):2073–2083, 2022.

[39] Jing Xin, Kemin Chen, Lei Bai, Ding Liu, and Jian Zhang. Depth adaptive zooming visual servoing for a robot with a zooming camera. *Int. J. Adv. Rob. Syst.*, 10(2):120, 2013.

[40] Chenguang Yang, Yiming Jiang, Jing Na, Zhijun Li, Long Cheng, and Chun-Yi Su. Finite-time convergence adaptive fuzzy control for dual-arm robot with unknown kinematics and dynamics. *IEEE Trans. Fuzzy Syst.*, 27(3):574–588, 2019.

[41] Xiaowei Yang, Wenxiang Deng, and Jianyong Yao. Neural adaptive dynamic surface asymptotic tracking control of hydraulic manipulators with guaranteed transient performance. *IEEE Trans. Neural Netw. Learn. Syst.*, pages 1–11, 2022.

[42] Jiazheng Zhang, Long Jin, and Yang Wang. Collaborative control for multimanipulator systems with fuzzy neural networks. *IEEE Trans. Fuzzy Syst.*, 31(4):1305–1314, 2023.

[43] Kunwu Zhang, Yang Shi, and Huaiyuan Sheng. Robust nonlinear model predictive control based visual servoing of quadrotor uavs. *IEEE/ASME Trans. Mechatronics.*, 26(2):700–708, 2021.

[44] Lina Zhang, Zhe Sun, Feng Duan, Chi Zhu, and Hiroshi Yokoi. Mind control of a service robot with visual servoing. In *Proc. IEEE/RSJ Int. Conf. Intell. Robots Syst. (IROS)*, pages 3747–3752, 2021.

[45] Yu Zhang, Changchun Hua, Yafeng Li, and Xinping Guan. Adaptive neural networks-based visual servoing control for manipulator with visibility constraint and dead-zone input. *Neurocomputing*, 332:44–55, 2019.

[46] Haodong Zhou, Shuai Sui, and Shaocheng Tong. Finite-time adaptive fuzzy prescribed performance formation control for high-order nonlinear multiagent systems based on event-triggered mechanism. *IEEE Trans. Fuzzy Syst.*, 31(4):1229–1239, 2023.

[47] Chengzhi Zhu, Yiming Jiang, and Chenguang Yang. Fixed-time neural control of robot manipulator with global stability and guaranteed transient performance. *IEEE Trans. Ind. Electron.*, 70(1):803–812, 2023.

[48] Chengzhi Zhu, Chenguang Yang, Yiming Jiang, and Hui Zhang. Fixed-time fuzzy control of uncertain robots with guaranteed transient performance. *IEEE Trans. Fuzzy Syst.*, 31(3):1041–1051, 2023.

Jiao Jiang received the B. E. degree in Electrical Engineering and Automation from China University of Mining and Technology, Xuzhou, China, in 2020. She is now working on her Ph.D. in Control Science and Engineering at the School of Electrical and Information Engineering, Hunan University, Changsha, China.

Her research interest covers robot vision perception and control.

Yaonan Wang(Senior Member, IEEE) received a Ph.D. degrees in electrical engineering from Hunan University, Changsha, China, in 1994. He was a Senior Humboldt Fellow in Germany from 1998 to 2000 and a Visiting Professor with the University of Bremen, Bremen, Germany, from 2001 to 2004. Dr. Wang is an Academician of the Chinese Academy of Engineering.

He is currently a Professor at the College of Electrical and Information Engineering, Hunan University. His research efforts mainly to robotics, image processing, and intelligent control.

Yiming Jiang Yiming Jiang received a Ph.D. degree in Pattern Recognition and Intelligent Systems from the South China University of Technology, Guangzhou, China, in 2019. He is an associate professor at the School of Robotics, Hunan University, and an associate research fellow at the National Engineering Research Center of Robot Visual Perception and Control Technology.

His research interest covers multiple robots' cooperative control and their application.

Yun Feng received the Ph.D. degree in Systems Engineering and Engineering Management, City University of Hong Kong, Hong Kong in 2020. He is currently an Associate Professor with the College of Electrical and Information Engineering, Hunan University, Changsha, China, and also with the National Engineering Laboratory for Robot Visual Perception and Control Technology, Hunan University, Changsha, China. His research interests include distributed parameter systems, fault diagnosis, and soft robotics. He was selected for the Young Elite Scientists Sponsorship Program by the China Association for Science and Technology in 2023.

Hang Zhong received the B.S., M.S., and Ph.D. degrees in automation science from the College of Electrical and Information Engineering, Hunan University, Changsha, China, in 2013, 2016, and 2020 respectively. From 2020 to 2022, he was a postdoc fellow with the College of Electrical and Information Engineering, Hunan University, Changsha, China. Now he is an Associate Professor with the College of Robotics, Hunan University. His research interests include aerial robotics, multi-robot systems, visual servoing, visual navigation and nonlinear control. He was a recipient of the Outstanding Doctoral Dissertation Award of Hunan Province in 2022.

Chenguang Yang (Senior Member, IEEE) received the Ph.D. degree in control engineering from the National University of Singapore, Singapore, in 2010, and postdoctoral training in human robotics from the Imperial College London, London, U.K. He was awarded UK EPSRC UKRI Innovation Fellowship and individual EU Marie Curie International Incoming Fellowship. As the lead author, he won the IEEE Transactions on Robotics Best Paper Award (2012) and IEEE Transactions on Neural Networks and Learning Systems Outstanding Paper Award (2022). He is the Corresponding Co-Chair of IEEE Technical Committee on Collaborative Automation for Flexible Manufacturing, a Fellow of Institute of Engineering and Technology (IET), a Fellow of Institution of Mechanical Engineers (IMechE), and a Fellow of British Computer Society (BCS). His research interest lies in human robot interaction and intelligent system design.